The Cryosphere

Modeling debris-covered glaciers: response to steady debris deposition

Leif S. Anderson[1] **and Robert S. Anderson**[2]

[1]Institute of Earth Sciences, University of Iceland, Askja, Sturlugötu 7, 101 Reykjavìk, Iceland
[2]Institute of Arctic and Alpine Research, and Department of Geological Sciences, University of Colorado, Campus Box 450, Boulder, Colorado, CO 80309, USA

Correspondence to: Leif S. Anderson (leif@hi.is)

Abstract. Debris-covered glaciers are common in rapidly eroding alpine landscapes. When thicker than a few centimeters, surface debris suppresses melt rates. If continuous debris cover is present, ablation rates can be significantly reduced leading to increases in glacier length. In order to quantify feedbacks in the debris–glacier–climate system, we developed a 2-D long-valley numerical glacier model that includes englacial and supraglacial debris advection. We ran 120 simulations on a linear bed profile in which a hypothetical steady state debris-free glacier responds to a step increase of surface debris deposition. Simulated glaciers advance to steady states in which ice accumulation equals ice ablation, and debris input equals debris loss from the glacier terminus. Our model and parameter selections can produce 2-fold increases in glacier length. Debris flux onto the glacier and the relationship between debris thickness and melt rate strongly control glacier length. Debris deposited near the equilibrium-line altitude, where ice discharge is high, results in the greatest glacier extension when other debris-related variables are held constant. Debris deposited near the equilibrium-line altitude re-emerges high in the ablation zone and therefore impacts melt rate over a greater fraction of the glacier surface. Continuous debris cover reduces ice discharge gradients, ice thickness gradients, and velocity gradients relative to initial debris-free glaciers. Debris-forced glacier extension decreases the ratio of accumulation zone to total glacier area (AAR). Our simulations reproduce the "general trends" between debris cover, AARs, and glacier surface velocity patterns from modern debris-covered glaciers. We provide a quantitative, theoretical foundation to interpret the effect of debris cover on the moraine record, and to assess the effects of climate change on debris-covered glaciers.

1 Introduction

Glaciers erode landscapes directly by subglacial quarrying and abrasion, and indirectly by steepening hillslopes above glaciers. Oversteepened hillslopes can deliver loose rock (debris) onto glacier surfaces (Benn and Evans, 2010). Steep hillslopes and high hillslope erosion rates in alpine settings therefore tend to correspond with the occurrence of debris-covered glaciers (e.g., the Himalaya and the Alaska Range). We refer to a debris-covered glacier as any glacier with continuous debris cover across the full glacier width over a portion of the glacier (after Kirkbride, 2011).

Debris cover more than a few centimeters thick damps the ablation of underlying ice (e.g., Østrem, 1959; Shroder et al., 2000; Owen et al., 2003). If debris supply to a glacier surface is high, mass balance profiles can be greatly altered, leading to increases in glacier volume and length (e.g., Konrad and Humphrey, 2000; Scherler et al., 2011a, b; Fig. 1). Thick debris cover on glaciers can also lead to low accumulation-area ratios (AARs; Scherler et al., 2011b). Estimates of past climate change will therefore be exaggerated if typical AARs are assumed when reconstructing past climate from moraines deposited by debris-covered glaciers.

Debris-covered glacier termini exhibit a wide range of responses to climate change (Scherler et al., 2011a). While almost all Himalayan debris-free glaciers are retreating, Himalayan debris-covered glacier termini are not respond-
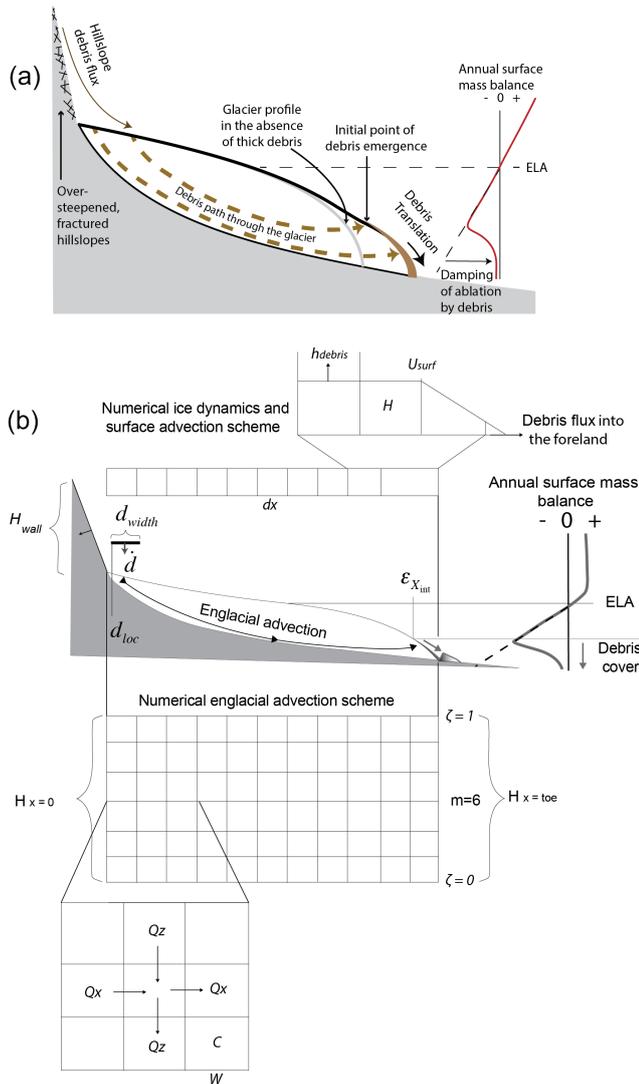
Figure 1. (a) Schematic of the debris–glacier system. Debris deposited on or emerging in the ablation zone reduces ablation rates (above the critical debris thickness) leading to the reduction in gradients of ice discharge and the lengthening of glaciers. **(b)** Schematic of the coupled debris–glacier model. Debris deposited on the glacier is either advected through the glacier and/or advected down the glacier surface. Englacial debris is advected using 2-D rectangular grid and coordinate transform. Ice physics and supraglacial debris advection is treated on a 1-D grid.

ing coherently to climate change despite a strong trend toward negative mass balance and surface lowering (e.g., Bolch et al., 2011, 2012; Benn et al., 2012; Kääb et al., 2012). Some Himalayan debris-covered glacier termini are advancing, others are stationary, and yet others are retreating (e.g., Raper and Braithwaite, 2006; Scherler et al., 2011a; Bolch et al., 2012). This discrepancy between debris-covered glacier mass balance and terminal response highlights the

pressing need to understand the sometimes counterintuitive effects of debris on glacier response.

The direct effect of debris on glaciers is difficult to isolate on modern glaciers. In situ documentation of debris-covered glacier mass loss is made difficult by non-uniform debris thicknesses and the presence of scattered ice cliffs, surface ponds, and proglacial lakes. As a result complete summer balances from debris-covered glaciers are sparse (WGMS, 2008). Measurements of englacial debris concentrations and distribution are yet more difficult to obtain (e.g., Kirkbride and Deline, 2013). In addition, exploration of century-scale response of debris-covered glaciers is limited by short satellite and observational periods (Bolch et al., 2011). Logistical realities therefore limit our ability to constrain feedbacks between debris deposition rates, the englacial environment, the supraglacial environment, and ice dynamics.

While logistics limit our ability to directly observe some feedbacks, many of the most provocative conclusions relating debris and glacier response are based on remotely sensed data. Scherler et al. (2011b) provided an extensive inventory of remotely sensed velocity and debris coverage data from 287 glaciers in High Asia. They inferred several general patterns from these debris-covered glaciers: (1) hillslope debris flux onto glaciers correlates with the percentage of debris cover on glaciers; (2) debris-covered glacier AARs tend to be smaller than debris-free glaciers; and (3) surface debris perturbs velocity distributions on valley glaciers by shifting maximum glacier velocities up glacier, away from the terminus. These inferences highlight the effect of thick debris cover on valley glaciers and serve as targets for models of debris-covered glaciers.

Numerical models can help quantify feedbacks within the debris–glacier–climate system (e.g., Konrad and Humphrey, 2000). Debris-covered glacier models have been used to explore the response of valley glaciers to (1) the steady input of debris (Konrad and Humphrey, 2000); (2) one-time landslide deposition of debris on glaciers (Vacco et al., 2010; Menounos et al., 2013); and (3) climate change (Naito et al., 2000; Banerjee and Shankar, 2013; Rowan et al., 2015). Konrad and Humphrey (2000) used a two-dimensional (2-D; long-valley-vertical) model with a constant surface slope to explore debris-covered glacier dynamics. In their model, debris was deposited on the glacier surface below the equilibrium-line altitude (ELA) and was then advected along the glacier surface. With high debris fluxes, simulated glaciers formed several-meter-thick debris covers, which reduced sub-debris melt toward zero, and resulted in glaciers that never reached steady state. Numerical models have also shown that large landslides onto glaciers can lead to multiple-kilometer advances of the terminus (Vacco et al., 2010; Menouonos et al., 2013). Debris-covered glacier retreat response timescales have also been explored with a simplified debris-covered glacier model (Banerjee and Shankar, 2013). Rowan et al. (2015) used a numerical model to forecast the response of the debris-covered Khumbu glacier,

Nepal to climate change. But owing to the complexity of the debris–glacier–climate system, it can be difficult to diagnose the effects of different processes on observable glacier responses. For example, both increased debris delivery to a glacier and a cooling climate could lead to glacier advances (e.g., Vacco et al., 2010; Menuounos et al., 2013). What approaches could we use to address these sorts of conundrums within the debris–glacier–climate system?

Here we attempt to improve our understanding of the debris–glacier–climate system (and subsequently better project future glacier change) by isolating how debris effects glacier response, while holding climate steady. While significant effort has focused on glacier-climate interaction, less research has focused on isolating the effect of debris on glacier length (e.g., Konrad and Humphrey, 2000), and other basic measures of glacier response (e.g., change in glacier surface velocity due to debris deposition on the glacier). We explore debris-glacier interactions by isolating the role of debris in governing basic glacier dynamics and glacier length.

We use a simple glacier model to simulate hypothetical debris-covered glaciers. This new framework allows us to isolate the effects of debris on glacier response by controlling the potentially conflating effects of a variable bed, variable glacier width, or a temporally variable climate. To isolate the effect of debris, we start each simulation with a steady state debris-free (ssdf) glacier and impose a step change increase in debris deposition rate while holding climate steady. In many debris-covered glacier systems, debris is deposited in the accumulation zone, advected through the glacier, and emerges in the ablation zone (e.g., Boulton and Eyles, 1979; Owen and Derbyshire, 1989; Benn and Owen, 2002; Benn et al., 2012). Our new transient 2-D numerical model (x, z) links debris deposition, englacial debris advection, debris emergence, surface debris advection, debris–melt coupling, debris removal from the glacier terminus, and shallow-ice-approximation dynamics (Figs. 1 and 2). We provide a new terminus parameterization which allows for the use of steady state glacier length as a metric for comparison between simulated debris-covered glaciers. While real debris-covered glaciers may not reach steady state the concept is necessary for determining the sensitivity of debris-covered glaciers to changes in debris-related parameters. Our intent is to determine which parameters and parameterizations are most important for capturing the response of glaciers to debris input. Here, we explore the sensitivity of hypothetical debris-covered glaciers to changes in debris-input related variables (e.g., debris flux, debris deposition location, and debris deposition zone width). We also explore the sensitivity of debris-covered glaciers to different debris thickness–melt formulations. We compare our theory-based results to the "general trends" documented by Scherler et al. (2011b). By isolating the effect of debris on glaciers, this study lays the theoretical foundation for efforts exploring the more complex response of debris-covered glaciers to climate change.
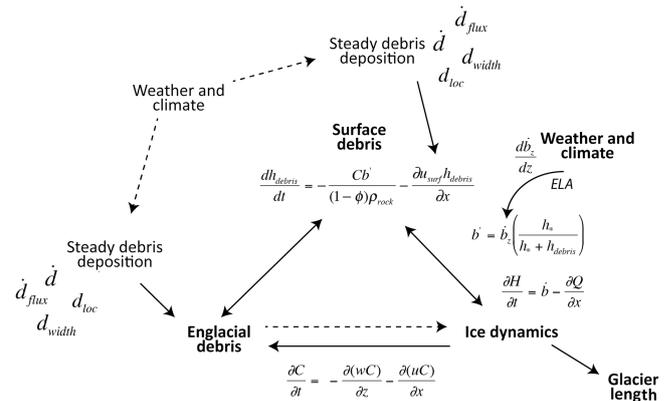
Figure 2. Flow chart of the elements connected in this debris-glacier model. Solid arrows represent the feedbacks we explore. Dashed arrows are neglected.

2 Theory and numerical methods

We employ a fully transient 2-D finite difference numerical model (in down-valley and vertical, x and z) that can simulate the evolution of temperate valley glacier response to climate and debris. Forced by a time series of equilibrium-line altitudes (ELAs) and a prescribed mass balance gradient, the model calculates ice surface elevations above a longitudinal profile by solving equations for ice flux and mass conservation. The modeled longitudinal path represents the glacier centerline. A number of authors have used the shallow-ice-approximation (SIA) and basal sliding parameterizations in numerical glacier models (e.g., Nye, 1965; Budd and Jensen, 1975; Oerlemans, 1986; MacGregor et al., 2000; Leysinger and Gudmundsson, 2004; Kessler et al., 2006). We employ a similar approach, but add a longitudinal stress coupling parameterization (Marshall et al., 2005). The model is efficient, allowing wide exploration of parameter space in simulations over thousands of years.

2.1 Conservation of ice mass

Mass conservation is at the core of the ice physics model. Assuming uniform ice density, and ignoring variations in the width of the glacier, ice conservation requires that

$$\frac{\partial H}{\partial t} = \dot{b} - \frac{\partial Q}{\partial x}, \tag{1}$$

where x is the distance along the glacier flowline, H is the local ice thickness, $\dot{b}$ is the local specific balance, and Q [in m^3 m^{-1} yr^{-1}] is the specific volume discharge of ice. This requires a prescribed mass balance field, and a prescription of the ice physics governing ice discharge.

2.2 Annual surface mass balance of ice in the absence of debris

We use a simple mass balance scheme that limits the number of parameters while honoring the essence of glacier surface mass balance. We combine surface accumulation and ablation into a single thresholded net mass balance profile as a function of elevation, z:

$$\dot{b}_z = \min\left(\frac{\mathrm{d}\dot{b}_z}{\mathrm{d}z}(Z_{\mathrm{ice}} - \mathrm{ELA}), \dot{b}_z^{\mathrm{max}}\right), \tag{2}$$

where $\frac{\mathrm{d}\dot{b}_z}{\mathrm{d}z}$ is the mass balance gradient with elevation, Z_{ice} is the ice surface elevation and $\dot{b}_z^{\mathrm{max}}$ is a maximum mass balance that accounts for the depletion of moisture available for precipitation at higher elevations. The annual surface mass balance of ice in the absence of debris is held steady for all simulations to isolate the effects of debris from those of climate change on glacier response.

2.3 Annual surface mass balance: effect of supraglacial debris

Sub-debris melt rate decreases rapidly with increasing debris thickness (e.g., Østrem, 1959; Nicholson and Benn, 2006). For debris layers thinner than a critical thickness (~ 2 cm), surface debris can increase melt rates relative to bare ice. For debris thicknesses greater than ~ 2 cm, debris suppresses sub-debris melt rates relative to bare ice (e.g., Nicholson and Benn, 2006; Fig. 3). We assume that heat is transferred through the debris layer by conduction. Sub-debris melt should therefore vary inversely with debris thickness (i.e., be hyperbolic) as conduction is governed by the temperature gradient $\sim (T_{\mathrm{s}} - T_{\mathrm{ice}})/h_{\mathrm{debris}}$ (e.g., Nicholson and Benn, 2006). Here, $T_{\mathrm{ice}} = 0$. We neglect the melt-amplifying effects of very thin debris for simplicity and represent the damping of sub-debris melt rates with

$$b' = \dot{b}_z\left(\frac{h_*}{h_* + h_{\mathrm{debris}}}\right), \tag{3}$$

where h_* is a characteristic length scale

$$h_* = \frac{k\overline{T}_{\mathrm{s}}}{(1-\phi)\rho_{\mathrm{i}}Lf_{\mathrm{pdd}}\overline{T}_{\mathrm{a}}}, \tag{4}$$

and k and ϕ are thermal conductivity and porosity of debris cover, ρ_{i} and L the density and latent heat of fusion of ice, $\overline{T}_{\mathrm{s}}$ the average debris surface temperature, $\overline{T}_{\mathrm{a}}$ the average screen-level air temperature, and f_{pdd} is a positive degree day factor relating air temperature and the bare ice melt rate (e.g., Mihalcea et al., 2006). In this formulation, sub-debris melt rates approach bare-ice melt rates as debris thins ($h_{\mathrm{debris}} \ll h_*$), and asymptotes toward a hyperbolic dependence on debris thickness as debris thickens ($h_{\mathrm{debris}} \gg h_*$). We use h_* values based on data from 15 studies (Fig. 3;
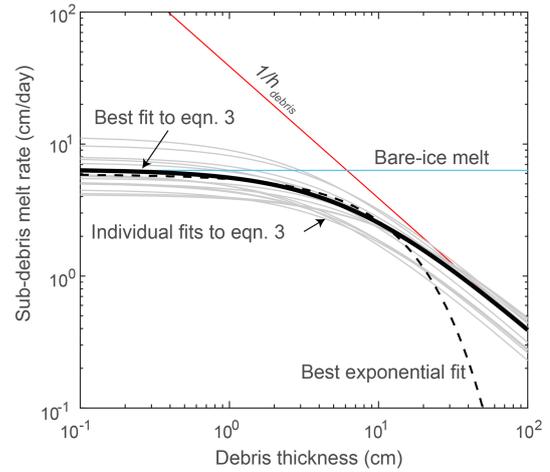
Figure 3. Compilation of curve fits to data from 15 melt rate vs. debris thickness studies (Østrem, 1959; Loomis, 1970; Khan, 1989; Mattson et al., 1993; Lundstrom, 1993; Kayastha et al., 2000; Lukas et al., 2005; Mihalcea et al., 2006; Nicholson and Benn, 2006; Hagg et al., 2008; Reid and Brock, 2010; Wang et al., 2011; Fyffe, 2012; Brook et al., 2013; Anderson, 2014) (mean h_* is 0.066 ± 0.029 m (1σ), and ranges from 0.03 to 0.13 m). These curve fits are used to determine the parameter ranges in Table 1 for h_*. The best exponential fit is the mean of all the exponential curve fits; using sub-debris melt $= ae^{\frac{-h_{\mathrm{debris}}}{b}}$ $a = 5.89$ cm day^{-1}, $b = 12.27$ cm.

$h_* = 0.066 \pm 0.029$ m (1σ), and ranges from 0.03 to 0.13 m). For comparison, we also show the most likely exponential fit to the data (Fig. 3). The exponential curve fit declines more rapidly than the hyperbolic fit (e.g., Konrad and Humphrey, 2000; Hagg et al., 2008). We neglect the effects of surface streams, thermokarst, and ice cliffs that can lead to complex local topography and melt rates within debris covers (e.g., Reid and Brock, 2014; Anderson, 2014).

2.4 Ice dynamics

Ice is transferred down valley by internal ice deformation and by basal motion. The ice discharge down glacier is

$$Q = H\overline{u}, \tag{5}$$

in which H is the local ice thickness and $\overline{u}$ is the depth-averaged bed parallel velocity that results from the sum of the ice deformation velocity and basal motion. The SIA reduces the momentum balance equations to expressions for vertical shear stress as a function of the local ice surface slope and ice thickness. The depth-averaged horizontal velocity due to internal deformation is

$$\overline{u}_{\mathrm{def}} = \frac{2A}{n+2}(\rho_{\mathrm{i}}g\alpha)^{n-1}H^n\tau_{\mathrm{b}x}, \tag{6}$$

where ρ_{i} the density of ice, g the acceleration due to gravity, α the local ice surface slope, H the local ice thickness, $\tau_{\mathrm{b}x}$ is the local basal shear stress, A is the creep parameter, and n is

the flow law exponent (assumed to be 3). We assume that all ice is temperate, and A is therefore taken to be 24×10^{-25} [in $Pa^{-3} s^{-1}$] (Cuffey and Paterson, 2010). In addition to internal deformation, temperate glaciers transfer mass via basal slip due to ice sliding over the bed and deformation of the bed itself. We assume that all basal slip is accomplished by sliding over bedrock, and follow the formulation of Kessler et al. (2006):

$$u_{\text{sliding}} = u_{\text{c}} e^{1 - \frac{\tau_{\text{c}}}{\tau_{\text{b}x}}} \tag{7}$$

in which u_{c} is a typical sliding velocity, and τ_{c} is the gravitational driving stress that gives rise to the typical sliding velocity. This sliding parameterization is not as sensitive to high τ_b values as many other sliding laws (e.g., Cuffey and Paterson, 2010), and provides a more conservative estimate of sliding velocities when $\tau_b > \tau_{\text{c}}$ (Kessler et al., 2006). We have also modified the SIA equations by including a parameterization of longitudinal stress coupling (after Marshall et al., 2005) and a shapefactor, f, that represents the effect of valley wall drag. The longitudinal coupling scheme modifies $\tau_{\text{b}x}$ to

$$\tau_{\text{b}x} = f \left(\rho_{\text{i}} g H \alpha + 4 \overline{\eta} H \frac{\partial^2 \overline{u}}{\partial x^2} + 4 \frac{\partial \overline{\eta} H}{\partial x} \frac{\partial \overline{u}}{\partial x} \right), \tag{8}$$

where the effective viscosity, $\overline{\eta} = \frac{1}{2} [A \tau_{\text{E}}^{n-1}]^{-1}$ and $\overline{u}$ is the vertically averaged ice velocity. In the shallow ice approximation, τ_{E}, the effective stress, is approximated by the local $\tau_{\text{b}x}$ (after Cuffey and Paterson, 2010). We take $f = 0.75$ to approximate the effects of sidewall drag from a parabolic valley cross-section with a half-width 3 times the ice thickness (Cuffey and Paterson, 2010).

2.5 Ice velocity structure within the glacier

Horizontal and vertical velocity fields must be resolved within the glacier in order to advect englacial debris. We start by defining the horizontal velocity field within the glacier, and then employ continuity in an incompressible medium to calculate the associated vertical velocities. The $u(z)$ profile shape may be obtained from the analytic solution to flow of ice in a uniform channel with Glen's flow law rheology:

$$F = 5 \left(\left(\zeta - 1.5 \zeta^2 \right) + \zeta^3 - \frac{1}{4} \zeta^4 \right), \tag{9}$$

where ζ is the non-dimensional height z/H above the bed, and $F = \frac{u(z)}{\overline{u}_{\text{def}}}$ is the ratio of horizontal speed to mean deformation speed. The full horizontal velocity field is then characterized by

$$U_\zeta(x, \zeta) = \overline{u}_{\text{def}}(x) F + u_{\text{sliding}}(x) + u_{\text{coupling}}(x), \tag{10}$$

where u_{coupling} is the vertically integrated velocity effect due to longitudinal stress coupling and is determined by subtracting the original Eq. (6) from Eq. (6) modified by Eq. (8).

Vertical and horizontal velocity fields ($w(x, z)$ and $u(x, z)$) are related through the continuity equation for an incompressible fluid, which in two dimensions (x, z) is

$$\frac{\partial w}{\partial z} = -\frac{\partial u}{\partial x}. \tag{11}$$

We then solve for the vertical velocity in each cell within each column by integrating vertically, as follows:

$$w = -\int_0^z \left(\frac{\partial u}{\partial x} \right) \mathrm{d}z, \tag{12}$$

employing the boundary condition that $w = 0$ at $z = 0$ (i.e., we assume no basal melt). In steady state, vertical velocities, w, at the glacier surface must be equal in magnitude and opposite in sign to the surface mass balance field, and are therefore directed downward at the ice surface in the accumulation zone, and upward in the ablation zone.

2.6 Debris deposition

Debris can be entrained in the glacier at the upper glacier surface, at the glacier bed, or along glacier sidewalls (e.g., Hambrey et al., 2008). Supraglacial debris deposition largely occurs by mass wasting from hillslopes above glaciers, while sub-glacial/sidewall debris entrainment occurs through regelation and net freeze-on. Basal debris emergence at the glacier surface is typically limited to the glacier toe and likely plays a minor role in the formation of extensive debris covers (Benn and Evans, 2010). We focus on debris sourced from valley head and side walls. Headwall erosion rates are better constrained than subglacial entrainment rates and mass wasting from head and sidewalls is the primary process of debris delivery onto many valley glaciers (Messerli and Zurbuchen, 1968; Humlum, 2000 (European Alps); Owen and Derbyshire, 1989 (Karakoram); Ballantyne and Harris, 1994; Humlum, 2000 (West Greenland); Benn and Owen, 2002 (Himalaya); Humlum, 2005 (Svalbard); Arsenault and Meigs, 2005 (Southern Alaska); O'Farrell et al., 2009 (Southern Alaska); Benn and Evans, 2010; Scherler et al., 2011b (High Asia)). The model replicates the deposition of debris onto the glacier surface leading to the formation of ablation-dominant and avalanche-type medial moraines on the glacier surface (Benn and Evans, 2010). For simplicity, we neglect englacial thrusting and ice-stream interaction moraines (medial moraines associated with tributary junctions; see Eyles and Rogerson, 1978; Anderson, 2000; Benn and Evans, 2010). These cases can be treated in subsequent modeling that incorporates the 2-D planform complexities of valley glaciers.

Debris delivery to glacier surfaces can vary considerably from glacier to glacier, depending on glacier topology and above-glacier topography (e.g., Deline, 2009). We capture this complexity using four variables: the total debris flux to

the glacier surface ($\dot{d}_{\text{flux}}$, [in $\text{m}^3\,\text{m}^{-1}\,\text{yr}^{-1}$]), the debris deposition rate ($\dot{d}$ [in $\text{mm}\,\text{yr}^{-1}$]), the debris deposition zone width (d_{width} [in m]), and the debris deposition location (d_{loc}). In the model, $\dot{d}_{\text{flux}}$ is representative of the integrated effects of $\dot{d}$ and d_{width}.

Rock type, slope, and fracture density are significant factors determining hillslope erosion rates and therefore also control the debris deposition rate, $\dot{d}$ (e.g., Stock and Montgomery, 1999; Molnar et al., 2007). In the model, $\dot{d}$, is allowed to vary from 1 to $8\,\text{mm}\,\text{yr}^{-1}$ and is steady within each simulation (Fig. 1b). Debris deposition rate depends on a number of site-specific variables:

$$\dot{d} = f_{\text{funneling}} f_{\text{hillslope}} \text{e} \frac{H_{\text{wall}}}{\tan(\theta)\text{d}x}, \qquad (13)$$

where $f_{\text{funneling}}$ is a dimensionless factor capturing the effect of topographic funneling on debris deposition, $f_{\text{hillslope}}$ is the percentage of the headwall that is exposed bedrock, e is the hillslope backwearing rate in $\text{m}\,\text{yr}^{-1}$, H_{wall} is the height of the headwall, and θ is the headwall slope. The deposition rates explored in this study are appropriate for typical headwall erosion rates (typically ranging between 0.5 and $2\,\text{mm}\,\text{yr}^{-1}$), headwall heights, and headwall slopes for high-relief mountain environments (e.g., Heimsath and McGlynn, 2008; Ouimet et al., 2009; Scherler et al., 2011; Ward and Anderson, 2011). d_{width} defines the down-valley width of the deposition zone, the zone over which the debris is spread on the glacier surface (we employ a base width of 400 m; Table 1; Fig. 1b).

Debris is deposited on glaciers at locations where hillslope erosion processes are connected to the glacier surface. This requires high-relief topography above the glacier to provide the energy necessary to move the debris onto the glacier. In the model, we control the down-valley debris deposition location with the variable d_{loc}, which we allow to vary from near the headwall to near the glacier terminus. d_{loc} defines the up glacier end of the debris deposition zone.

2.7 Incorporation and advection of englacial debris

Debris deposited in the ablation zone is advected along the glacier surface, whereas debris deposited in the accumulation zone moves downward with the ice and is therefore incorporated into the glacier. The near-surface debris concentration in the accumulation zone is defined as $C_0 = \frac{\dot{d}\rho_{\text{rock}} m_z \text{d}t}{H}$, where m_z is the number of vertical slices the englacial advection scheme is divided into (H/m_z being the thickness of the slices) and dt is the model time interval. C_0 is therefore the mass concentration of debris in the surface-bounding cell.

Once embedded in the glacier, debris is advected through the glacier following englacial flowpaths ($\frac{\partial C}{\partial t} = -\frac{\partial(uC)}{\partial x} - \frac{\partial(wC)}{\partial z}$). Taking an Eulerian point of view, the time rate of change of concentration of debris within an ice cell (in our

model) is

$$\frac{\partial C}{\partial t} = -\frac{\partial(uC)}{\partial x} - \frac{\partial(wC)}{\partial z} - \frac{C}{h_\zeta}\frac{\partial h_\zeta}{\partial t} - \frac{uC}{h_\zeta}\frac{\partial h_\zeta}{\partial x}, \qquad (14)$$

where h_ζ is the cell height in a given ice column ($h_\zeta = \frac{H}{m_z}$). The first and second terms represent changes in C due to advection in the vertical and the horizontal directions, respectively. The third term on the right hand side represents the rate of change of C due to vertical ice strain from the thinning or thickening of the glacier through time. Note that if the strain rate is negative, signifying vertical thinning of an ice column, debris concentration in a cell will increase. The fourth term represents the rate of change of C due to the longitudinal changes in glacier thickness. This term accounts for the fact that cells from one column to the next are not the same volume.

2.8 Advection of debris on the glacier surface and steady states

We track both the melt-out of englacial debris and the advection of supraglacial debris on the glacier surface. The rate of change of debris thickness on the glacier surface is captured by

$$\frac{\text{d}h_{\text{debris}}}{\text{d}t} = -\frac{Cb'}{(1-\phi)\rho_{\text{rock}}} - \frac{\partial u_{\text{surf}}h_{\text{debris}}}{\partial x}, \qquad (15)$$

where h_{debris} is the debris thickness, ρ_{rock} is the density of the rock, ϕ is the porosity of supraglacial debris, and u_{surf} is the surface velocity of the glacier (after Konrad and Humphrey, 2000; Naito et al., 2000; Vacco et al., 2010). The first term on the right represents the addition of debris to the surface from melt of debris-laden ice. The second term represents the advection of debris down glacier.

Debris is transported off glacier by the wasting of debris down the terminal slope or by the backwasting of terminal ice cliffs (Konrad and Humphrey, 2000; Appendix A and B). In the model we implement a triangular terminus wedge parameterization (after Budd and Jenssen, 1975; see Appendix A). The change of surface debris thickness with time on the terminal wedge is

$$\frac{\text{d}h_{\text{debris}}^{\text{term}}}{\text{d}t} = -\frac{\dot{d}_{\text{flux}}^{\text{term}}}{\text{d}x_{\text{term}}} - \frac{Cb'}{(1-\phi)\rho_{\text{rock}}} - \frac{\partial u_{\text{surf}}h_{\text{debris}}}{\partial x}, \qquad (16)$$

where $\dot{d}_{\text{flux}}^{\text{term}}$ is the debris flux into the foreland from the terminus wedge [in $\text{m}^3\,\text{m}^{-1}\,\text{yr}^{-1}$] and d$x_{\text{term}}$ is the surface length of the terminal wedge. We use $\dot{d}_{\text{flux}}^{\text{term}} = \dot{b}_z^{\text{term}} h_{\text{debris}}^{\text{term}}$. Varying this parameterization has a minor effect on glacier length, but can have a considerable effect on the temporal evolution of the glacier as $\dot{d}_{\text{flux}}$ must equal $\dot{d}_{\text{flux}}^{\text{term}}$ for a simulated glacier to reach steady state (Appendix A). We explore the choice and effect of this parameterization in Appendix B.

Table 1. Parameter definitions and values.

Parameter	Name	Min	Base	Max	Units
ELA	Equilibrium-line altitude		5000		m
$\frac{d\dot{b}_z}{dz}$	Surface mass balance gradient		0.0075		yr^{-1}
$\dot{b}_z^{max}$	Maximum balance		2		$m\,yr^{-1}$
Z_{max}	Maximum bed elevation		5200		m
α	Bed slope	4 %	8 %	20 %	
dt	Time step		0.01		yr
dx	Down-valley spatial discretization		100	200	m
dy	Valley perpendicular spatial discretization		1		m
g	Gravity		9.81		ms^{-2}
n	Glen's constant		3		
A	Flow law parameter		2.4×10^{-24}		$Pa^{-3}\,yr^{-1}$
f	Shapefactor		0.75		
U_c	Critical sliding speed		5		$m\,yr^{-1}$
τ_c	Reference basal shear stress		10^5		Pa
ρ_{ice}	Ice density		917		$kg\,m^{-3}$
m_z	# of cells per ice column		20		
ρ_{rock}	Debris density		2650		$kg\,m^{-3}$
h_*	Characteristic debris thickness	0.025	0.065	0.165	m
ϕ	Surface debris porosity	0.18	0.3	0.43	
$\dot{d}$	Debris deposition rate	1	8	8	$mm\,yr^{-1}$
d_{loc}	Debris deposition location	7 %	42 %	98 %	
d_{width}	Debris deposit width	100	400	1600	m
$\dot{d}_{flux}$	Debris flux onto the glacier	0.1	3.2	6.4	$m^3\,m^{-1}\,yr^{-1}$
$\dot{d}_{flux}^{term}$	Debris flux off the glacier				$m^3\,m^{-1}\,yr^{-1}$
L_{ssdf}	Steady state debris-free glacier length		8700		m

3 Implementation and numerics

We now outline the order of calculations in the model. First, $\dot{b}_z$ and b' are calculated based upon elevation and debris thickness. Next, we use a second-order Runge–Kutta centered difference scheme to evolve $H(x, t)$, followed by the implementation of an iterative "upstream" debris advection scheme following Smolarkiewicz, 1983. This iterative scheme imposes a two-step anti-diffusion correction algorithm to the advection scheme, which greatly reduces numerical diffusion (Smolarkiewicz, 1983). We test advection scheme stability using the Courant–Friedrichs–Lewy (CFL) condition, which ensures that mass is not advected beyond adjacent cells in a single timestep. We implement a terminus wedge parameterization that allows simulated glaciers to advance to steady state (Appendix A and B). The time step, dt, for ice-physics and debris advection is 0.01 years. All ice columns are segmented into m_z heights (i.e., $\zeta = 0 : (1/m_z) : 1$); in all results below we use $m_z = 20$ (Fig. 1b). We impose a no-flux boundary at the upper end of the glacier.

While our simulations are hypothetical we select the base model parameters to loosely represent the ablation zones of debris-covered glaciers in the Khumbu region of Nepal. There is a wealth of debris-covered glacier research from this region, which assures that our parameter choices in the range of observed values (e.g., Kayastha et al., 2000; Bolch et al., 2011; Benn et al., 2012; Shea et al., 2015). Base simulations are run on a linear glacier bed with a basal slope of 8 % and a maximum bed elevation of 5200 m (Scherler, 2014). This simple bed geometry is used to ensure that our results to do not conflate the effects of bed topography with the effects of debris. We use a $\frac{d\dot{b}}{dz} = 0.0075\,yr^{-1}$, which is capped at $2\,m\,yr^{-1}$ based on data from debris-free glaciers in the Khumbu region (Mera and Pokalde glaciers: after Wagnon et al., 2013). Our parameter exploration below shows that our conclusions are not influenced by our choice of base parameters from the ablation zones of debris-covered glaciers in the Khumbu region. All simulations start with an 8.7 km long steady state debris-free (ssdf) glacier with a steady ELA at 5000 m ($L_{ssdf} = 8.7$ km). In each simulation a step change increase in debris deposition rate is imposed at $t = 100$ years. The base parameter set uses $\dot{d}_{flux} = 3.2\,m^3\,m^{-1}\,yr^{-1}$, $\dot{d} = 8\,mm\,yr^{-1}$, d_{width} of 400 m, and the location of debris input, d_{loc}, is 42 % of the distance between the headwall and the length of the debris-free glacier, L_{ssdf}.

4 Numerical experiments and results

We first demonstrate the transfer of debris between model components and demonstrate debris-covered steady state. We then explore the differences between the steady state debris-free (ssdf) glacier and debris-covered glaciers and explore relative importance of $\dot{d}$, d_{width}, d_{loc}, $\dot{d}_{\text{flux}}$, and $\dot{d}_{\text{flux}}^{\text{term}}$ on glacier length. The effect of $\dot{d}_{\text{flux}}^{\text{term}}$ on the length and time evolution of the model is explored in Appendix B (see Fig. B1). We then test the sensitivity of the model to changes in h_* and ϕ. Last, we compare our hypothetical simulations to "general trends" observed from real debris-covered glaciers.

4.1 Demonstration of debris-covered glacier steady state and conservation of debris

In order to compare steady state glacier lengths between simulations with different $\dot{d}_{\text{flux}}$ we track debris through the model. At any time in the simulation, the total debris mass that has been deposited on the simulated glacier must equal the total debris mass in the model:

$$M_{\text{input}} = M_{\text{englacial}} + M_{\text{surface}} + M_{\text{foreland}}, \qquad (17)$$

where M_{input} is the total rock mass deposited on the glacier and accumulated over time, $M_{\text{englacial}}$ is the total englacial debris mass, M_{surface} is the total debris mass on the glacier surface, and M_{foreland} is the total mass deposited in the proglacial environment.

We use the base parameter set simulation to highlight the transfer of debris mass through the system (Fig. 4). Because debris is deposited in the accumulation zone near the ELA, in the base simulation, $M_{\text{englacial}}$ rapidly reaches steady state (Fig. 4). As the glacier extends, M_{surface} continues to increase at a declining rate as more surface debris is transferred into the foreland. The glacier reaches steady state when the glacier length, M_{surface}, and $M_{\text{englacial}}$ are steady and the rate of change of M_{foreland} is equal the rate of debris input to the glacier. Each model simulation presented conserves greater than 99 % of debris mass.

4.2 Comparison of modeled debris-free and debris-covered glaciers

We first highlight differences in length, and the patterns of ice discharge, Q, ice thickness, H, and surface speed, u_{surf}, between the ssdf glacier and its steady state debris-covered counterpart, using the base parameter set (Fig. 4). In this baseline case the steady state debris-perturbed glacier length is 175 % of L_{ssdf} (Fig. 5).

The debris thickness, h_{debris}, increases down glacier from the site of debris emergence, $x_{\epsilon_{\text{int}}}$, except near the terminal wedge where the $\dot{d}_{\text{flux}}^{\text{term}}$ parameterization reduces h_{debris} (Figs. 5–6). Down glacier from the site of debris emergence, $x_{\epsilon_{\text{int}}}$, gradients of Q, H, and u_{surf} are reduced relative to the debris-free glacier (Fig. 6b and d). Debris-free patterns of
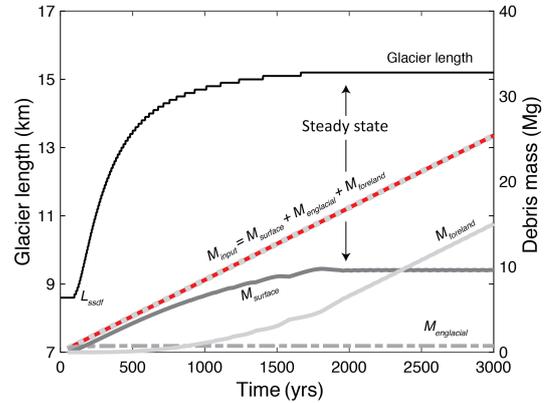
Figure 4. Debris mass vs. time. The englacial debris mass reaches steady state rapidly because debris is deposited near the ELA and englacial advection paths are short. As debris emerges in the ablation zone M_{surface} increases nearly at the rate of debris input to the glacier. As the glacier nears a steady length the debris mass transferred to the glacier foreland increases. The glacier reaches steady state when $\dot{d}_{\text{flux}} = \dot{d}_{\text{flux}}^{\text{term}}$ and the glacier length is steady (see Appendix A).
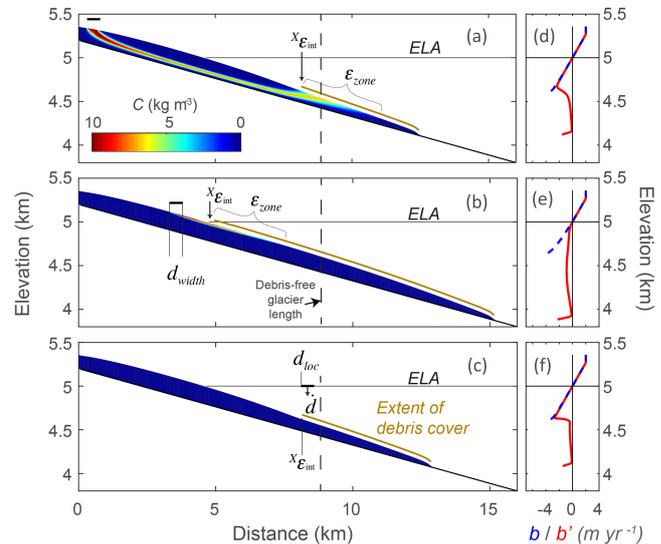
Figure 5. Modeled glacier changes due to changes in debris deposition location with debris flux held constant. Englacial debris concentrations **(a–c)** and mass balance profiles **(d–f)** for three steady state debris-covered glacier simulations. $\dot{d}_{\text{flux}} = 3.2 \, \text{m}^3 \, \text{m}^{-1} \, \text{yr}^{-1}$ for each panel. **(a)** d_{loc} is 7 % of the steady state debris free glacier length (L_{ssdf}) from the head of the glacier. **(b)** d_{loc} is 42 % to L_{ssdf}. **(c)** $d_{\text{loc}} = 98 \%$ to L_{ssdf}. The increase in melt rate near the toe is related to the thinning of debris due to the $\dot{d}_{\text{flux}}^{\text{term}}$ parameterization. $x_{\epsilon_{\text{int}}}$ is the point of initial debris emergence and ϵ_{zone} is the length of the glacier over which englacial debris emerges.
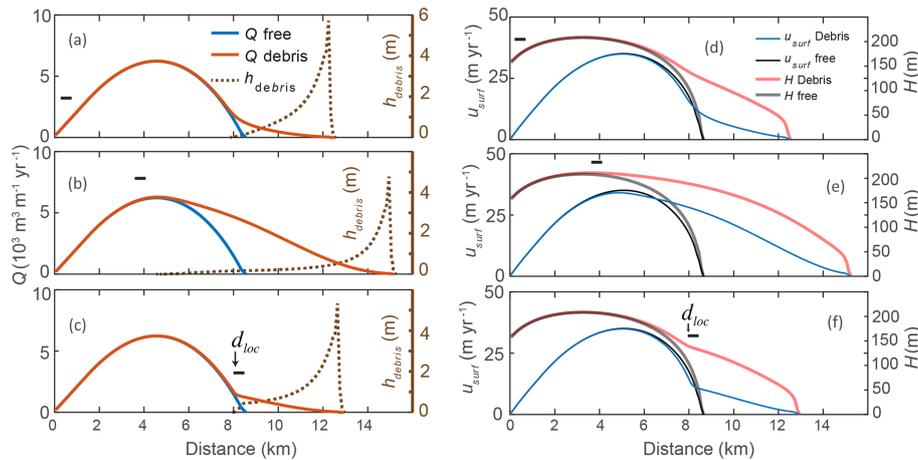
Figure 6. Modeled changes in ice fluxes, thicknesses and velocities due to debris deposition location. $\dot{d}_{flux} = 3.2\,\mathrm{m^3\,m^{-1}\,yr^{-1}}$ for each panel and other parameters excluding d_{loc} are from the base set. **(a–c)** Comparison of h_{debris} and Q for the debris covered and debris free cases shown in Fig. 6. **(d–f)** Comparison of surface velocities and ice thicknesses for the debris covered and debris-free cases. **(a)** d_{loc} is 7 % from the headwall to the steady state debris free glacier length (L_{ssdf}). **(b)** d_{loc} is 42 % from the headwall to L_{ssdf}. **(c)** d_{loc} is 98 % from the headwall to L_{ssdf}. **(d)** d_{loc} is 7 % from the headwall to L_{ssdf}. **(e)** d_{loc} is 42 % from the headwall to L_{ssdf}. **(f)** d_{loc} is 98 % from the headwall to L_{ssdf}.

Q and u_{surf} are convex up near the glacier terminus, while Q and u_{surf} from debris-covered termini are concave upward. The lowest gradients in Q, H, and u_{surf} occur near the glacier terminus where h_{debris} is thickest (excluding the terminal slope; Fig. 6).

4.2.1 Effect of debris input location

Debris input location (d_{loc}) controls the englacial debris path. Debris deposited near the headwall is advected more deeply into the glacier than debris deposited near the ELA. Debris deposited near the ELA follows a shallow, short englacial path (Fig. 5). The original width of the debris band deposited in the accumulation zone, is reduced down glacier and then widens again near the surface in the ablation zone (Fig. 5). The debris band initially narrows due to the longitudinal straining of ice (Hooke and Hudleston, 1978; Cuffey and Paterson, 2010; Fig. 5a) and then widens due to feedbacks between the surface debris and ice dynamics.

In order to show the effects of d_{loc} on basic glacier properties (glacier length, Q, H, and u_{surf}), we highlight three simulations where we vary d_{loc} and hold all other debris-related parameters constant ($\dot{d}_{flux} = 3.2\,\mathrm{m^3\,m^{-1}\,yr^{-1}}$, $\dot{d} = 8\,\mathrm{mm\,yr^{-1}}$, and $\dot{d}_{width} = 400\,\mathrm{m}$). d_{loc} is varied from near the top of the glacier to near the debris-free glacier toe (Figs. 5 and 6).

When debris is deposited or emerges where Q is large (near the ELA), glacier extension is greater than when debris is deposited/emerges where Q is small (near the headwall or the debris-free glacier terminus). If debris is deposited or emerges where Q_{free}/Q_{max} nears 1 glacier extension will be largest for a given glacier (Q_{free} refers to ice discharge from

the ssdf glacier and Q_{max} is the maximum Q_{free} before debris is added to the glacier). Where Q_{free}/Q_{max} nears 0 glacier extension will be small.

We ran an additional 33 simulations (36 total) in which we vary $\dot{d}_{flux}$ and d_{loc} (Fig. 7). Varying the debris deposition location while holding the debris flux constant results in a maximum of a 40 % difference (for these 36 simulations; Table 2) in the resulting steady-state debris-covered glacier length. The importance of d_{loc} on glacier length increases with larger $\dot{d}_{flux}$ (Fig. 7). The general pattern seen in Fig. 7 is insensitive to changes in other parameters. Increasing $\dot{d}_{flux}$ leads to increases in the percentage of the glacier covered with debris (Fig. 8).

4.2.2 Effect of debris deposition rate, debris deposit width, and debris flux

Increasing either the debris deposition rate ($\dot{d}$) or the debris deposit width (d_{width}) leads to increases in $\dot{d}_{flux}$, but the relative importance of $\dot{d}$ or d_{width} in governing glacier response is unclear. Does debris delivered to a small portion of a glacier at a high rate lead to a different length response than debris delivered to a glacier in a wide section but at a low rate? In order to parse the effects of $\dot{d}$ and d_{width} on glacier length, we ran simulations in which we vary $\dot{d}$ and d_{width} (Fig. 9b for $d_{loc} = 42\%$). The effect is small, varying the contribution results in a maximum of a 4 % difference in steady-state debris-covered glacier length for any given debris flux (Fig. 9b; Table 2). In contrast, varying the debris flux, $\dot{d}_{flux}$, results in a maximum of 80 % change in glacier length (Fig. 9c; Table 2).

Table 2. Sensitivity of steady state glacier length to changes in debris-related parameters.

Parameter	Name	Max. % length change relative to L_{ssdf}
h_*	Characteristic debris thickness	110 %
$\dot{d}_{\text{flux}}$	Debris flux onto the glacier	80 %
d_{loc}	Debris deposition location	40 %
ϕ	Surface debris porosity	25 %
$\dot{d}_{\text{flux}}^{\text{term}}$	Debris flux off the glacier	25 %*
$\dot{d}$ vs. d_{width}	Debris deposit location vs. width	4 %

* results from the $\dot{d}_{\text{flux}}^{\text{term}} = c\dot{b}h_{\text{debris}}$ parameterization.
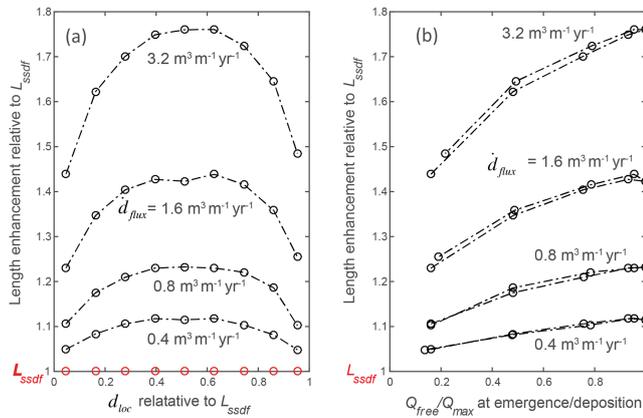
Figure 7. Glacier length variations with changes in debris flux($\dot{d}_{\text{flux}}$) and debris deposition location(d_{loc}). Modeled glacier length is normalized by the steady state debris free glacier length (L_{ssdf}). Each string of connected markers represents simulations with the same debris flux ($\dot{d}_{\text{flux}}$). Changes in $\dot{d}_{\text{flux}}$ are accomplished by changing $\dot{d}$ with d_{width} held constant. The red markers indicate the ssdf glacier length. **(a)** Normalized glacier length relative to d_{loc}. **(b)** Normalized glacier length relative to $Q_{\text{free}}/Q_{\text{max}}$ at the point of debris emergence/deposition.

Figure 8. Debris-related results from 36 simulations varying d_{loc} and $\dot{d}_{\text{flux}}$. All black circles are derived from steady state debris-covered glaciers. Red circle shows results from the debris-free glacier. Dashed lines connect simulations with the same d_{loc}.

4.3 Effect of characteristic debris thickness and surface debris porosity

We explore the sensitivity of the model to changes in the characteristic debris thickness (h_*) and surface debris porosity (ϕ). We vary h_* and ϕ, impose a step change increase in debris input to the ssdf glacier and compare the resulting steady state glacier lengths (Fig. 10). Simulated glacier length is highly sensitive to h_* (Fig. 10). For the same debris delivery variables, the more rapidly the melt rate is damped by debris (lower h_*), the longer the steady state glacier. Steady state debris-covered glacier length varies by 110 % relative to L_{ssdf} when h_* is varied from the extremes of 0.0035 to 0.165 m (Table 2; 55 % for the 1 σ range (0.037–0.095 m)). Glacier length is not as sensitive to the choice of debris porosity, ϕ (Fig. 10). Varying ϕ between the extremes of 0.18 and 0.43 (e.g., Bozhinskiy et al., 1986; Conway and

Rasmussen, 2000) leads to lengths that vary 25 % relative to L_{ssdf} (Table 2).

4.4 Comparison with trends observed from debris-covered glaciers

Our model results show that steady, high debris fluxes onto glaciers lead to increased glacier lengths and high percentages of debris cover (Figs. 8 and 9). Remote-sensing derived measurements provide general insight into valley glacier response to debris. We compare our hypothetical results to the broad trends Scherler et al. (2011b) inferred from their inventory of 287 debris-covered glacier surface velocity patterns, AARs, and debris cover percentages. While the Scherler data set was collected from glaciers responding to persistent negative mass balance, the authors note that their inferences stand even "when excluding stagnating glaciers". This suggests that their observations represent "general trends" relating debris to glacier response (e.g., increasing debris flux leads to reduced AARs and an up glacier shift of maximum glacier surface velocities).
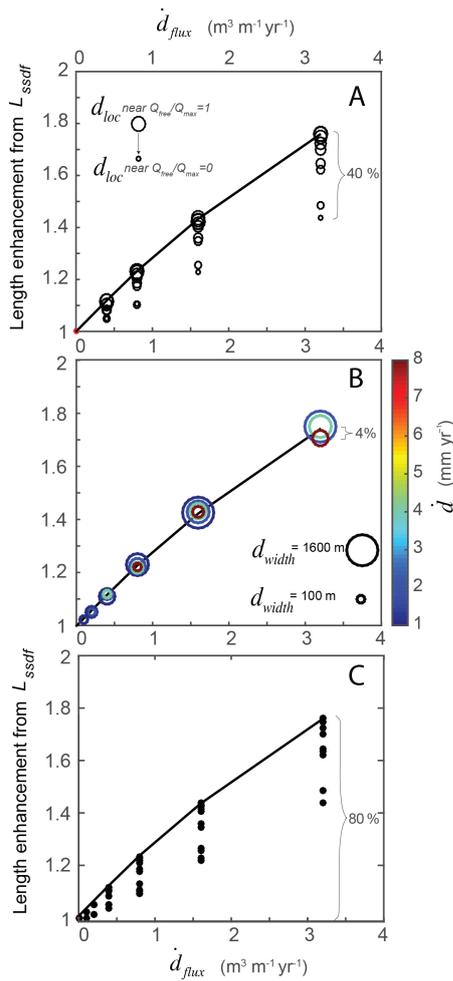
Figure 9. Dependence of steady state glacier length on debris delivery to the glacier. Glacier lengths are normalized by the steady state debris free glacier length, L_{ssdf}. Bold lines connect results with the same location of debris input, with d_{loc} fixed at 42 %. **(a)** Steady state glacier lengths from simulations in which debris flux, $\dot{d}_{flux}$ and d_{loc} are varied, and d_{width} is fixed at 400 m. Vertical columns of points represent simulations in which debris location is varied and debris flux is held constant. The same results are presented in Fig. 7. **(b)** Steady state glacier lengths from simulations in which $\dot{d}_{width}$ and $\dot{d}$ are varied while d_{loc} remains fixed at 42 %. The diameter of circle represents width of the debris deposition zone, its center representing the steady state glacier length. Clusters of circles are simulations with the same debris flux. **(c)** Steady state glacier length from all simulations in **(a)** and **(b)** in which, d_{width}, $\dot{d}$, and d_{loc} are varied. The maximum effect of varying $\dot{d}_{flux}$ on steady state glacier length is 80 %.

Scherler et al. (2011b) documented that higher debris cover percentage on glaciers correlates with steep above-glacier hillslopes. Because hillslope erosion rates and the percentage of exposed bedrock in the headwall increase with steeper slopes, it follows that increased debris input onto a glacier should also increase both the glacier length and the
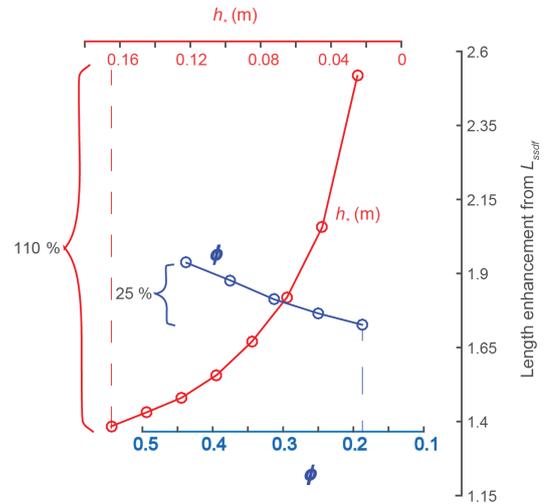
Figure 10. Sensitivity of steady state debris-covered glacier length to choices of characteristic debris thickness (h_*) and surface debris porosity (ϕ). The lines intersect at the base parameter set. Parameter ranges are extreme to highlight the possible range of effects of each parameter.

percentage of the glacier covered with debris. Our hypothetical model results confirm this inference and show that – independent of parameter selection (e.g., d_{loc}, h_*, bed slope) – higher debris flux leads to higher debris cover percentages on glaciers (Figs. 8 and 11).

Scherler et al. (2011b) showed that large debris cover percentages correspond with small AARs outside the typical range of 0.5–0.7 from debris-free glaciers (e.g., Meier and Post, 1979). Our modeled steady state debris free glacier has an AAR of 0.5 (due to the piecewise-linear mass balance profile and constant width valley). In our model simulations, increases in debris flux lead to increases in both steady state glacier length, and debris cover percentage independent of parameter selection (Fig. 11a). With a fixed ELA, the AAR must therefore decrease with an increased debris flux (Fig. 11a). Varying h_* (using the base parameter set; Fig. 10) has a similar effect to varying debris flux (Fig. 11c and d). Changes in the location of debris input lead to small changes in AAR but considerable changes in debris cover percentage (Fig. 11a).

Scherler et al. (2011b) also showed that larger debris cover percentage correlated with lower ratios of average surface speed(u_{surf}) from the lower half of glaciers to the average u_{surf} from the upper half of glaciers. Increasing the debris flux in our model leads to lower u_{surf} in the lower half of glaciers relative to u_{surf} in the upper half of glaciers independent of parameter selection (Fig. 11b). Changing the location of debris input, d_{loc}, leads to small changes in the ratio of average u_{surf} but leads to large changes in the percentage of the glacier covered with debris. This highlights that debris flux
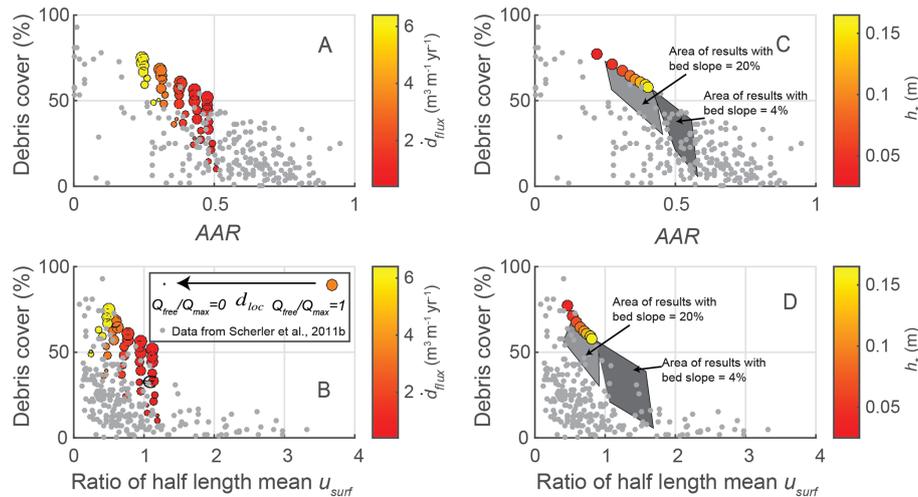
Figure 11. Comparison of our hypothetical steady state debris-cover model output with data from 287 glaciers showing broad patterns between debris and basic glacier properties (Scherler et al., 2011b). **(a)** The AAR compared to debris cover percentage, debris flux ($\dot{d}_{\text{flux}}$), and debris deposition location (d_{loc}). **(b)** The ratio of the average surface speed of the lower 50 % of the glacier and the average surface speed of the upper 50 % of the glacier vs. debris cover percentage, $\dot{d}_{\text{flux}}$, and d_{loc}. **(c, d)** Same data as **(a, b)**, but exploring the effect of changing the bed slope and h_*. The quadrangles show the area occupied by simulation results using the same parameters from **(a, b)** but with lower and higher bed slopes. h_* results are from the parameter test where h_* is varied (Fig. 10).

and debris deposition location are important parameters for the specific response of a glacier to debris input.

In order to show the generality of inferences made by Scherler et al. (2011b), we also change the bed slope in our hypothetical model. Changing the linear bed slope leads to similar relationships between debris cover percentage, AAR, and surface velocity. Notable differences occur primarily when the bed slope is reduced (Fig. 11c and d). With a reduced bed slope the initial debris-free steady state glacier is 3 times longer than the steady state debris free glacier. Even with the same hillslope debris fluxes as the simulations in Fig. 11a and b, the reduced bed slope leads to reduced asymmetry in the steady state debris-covered glacier surface velocities (Fig. 11d). With a linear mass balance profile and linear bed slope, changing the bed slope will have a similar effect to changing the mass balance gradient. The specific relationship of glacier response to debris is therefore also dependent on glacier size, bed slope, and the environmental mass balance gradient. Ultimately, our exploration shows that, independent of parameter selection (e.g., not dependent on bed slope or mass balance profile selection), our model reproduces basic patterns inferred from real debris-covered glaciers, which lends support to our model framework, while also providing quantitative, theoretical support to previous data-based observations.

5 Discussion

We explored the sensitivity of a new debris-covered glacier model to changes in various parameters and debris input related variables. We used a rigorous steady state glacier length

definition to allow for the intercomparison of each simulation. Simulated glacier lengths are most sensitive to hillslope debris flux and the selection of the debris thickness that characterizes the decline in melt rate beneath debris (Table 2). The location of debris deposition is important but plays a secondary role in setting glacier length. The time evolution of debris-covered glacier length is highly dependent on $\dot{d}_{\text{flux}}^{\text{term}}$, although steady state glacier length is not (Appendix B; Fig. B1). Thick debris cover on glaciers from consistent debris input, independent of climate change, tends to (1) reverse and reduce mass balance gradients; (2) extend glaciers; (3) reduce AARs; and (4) reduce gradients of ice discharge, ice thickness, and surface velocity under debris cover. Independent of parameter selection, our simulations reproduce general relationships between debris cover percentages, AAR, and debris-perturbed surface velocity patterns from debris-covered glaciers.

5.1 The importance of debris flux and characteristic debris thickness on steady state glacier length

Increases in hillslope debris flux ($\dot{d}_{\text{flux}}$) lead to glacier extension (Figs. 8 and 9; Scherler et al., 2011b). But the rate and location of debris delivery to the surface will vary widely due to local geologic and climatic settings. Our simulations show that debris flux is more important in determining the steady state debris-covered glacier length than $\dot{d}$, d_{loc}, or d_{width} (Fig. 9; Table 2). Processes of debris delivery to the glacier surface (e.g., deposition by avalanches, rockfall, the melt out of debris septa forming ice-stream interaction medial moraines, etc.) are first-order controls on the geometry

of debris deposits on glaciers. Because debris flux trumps the importance of $\dot{d}$, d_{loc}, and d_{width}, the specific debris delivery pathway is secondary to the debris flux in determining glacier length at least for this 2-D case.

The effects of changing h_* are similar to the effects of varying the hillslope debris flux (Figs. 10 and 11). Establishing the importance of debris flux for individual glaciers requires that we constrain the variability of h_* from glacier to glacier: small changes in h_* can lead to large changes in steady state glacier length (Fig. 10). Simulations using an exponential debris thickness–melt curve (e.g., Konrad and Humphrey, 2000; Hagg et al., 2008) resulted in unrealistically long glaciers due to the rapid asymptote of melt towards zero (see Fig. 3). We argue that the hyperbolic parameterization (Eq. 3) is more physically defensible than the exponential, as we assume that heat transfer through debris is dominated by conduction.

Many paleoclimate estimates derived from glacial moraines neglect the potential effects of surface debris. Because debris strongly influences glacier length, independent of climate change, debris should be considered amongst temperature and precipitation as primary controls of paleoglacier lengths (e.g., Clark et al., 1994; Scherler et al., 2011b). The effect of debris on paleoclimate estimates can be minimized by avoiding de-glaciated catchments with high-relief headwalls, supraglacially sourced moraine sediments, or by using a debris–glacier–climate model to estimate the effect of debris on glacier extent.

5.2 The effect of steady debris input on patterns of Q, H and u_{surf}

In all debris-perturbed simulations, the mass balance gradient down glacier from the location of initial debris emergence, $x_{\epsilon_{int}}$, reverses relative to the debris-free profile, decreases toward zero, and becomes more uniform (excluding the terminal wedge; Fig. 5). This reversal results in a reduction of the surface mass balance b' relative to the steady-state debris free glacier (Fig. 6). Reducing b' toward zero reduces ice discharge gradients leading to glacier extension.

Thick debris reduces b' toward 0 and also makes b' more uniform (Fig. 5). This leads to ice discharge gradients that are reduced toward zero and become more uniform near the terminus (Fig. 5). Because $Q = H\overline{u}$, the surface velocity pattern follows a similar concave up pattern near the terminus where ice thicknesses are small and b' is close to zero (Fig. 6). Low ice thicknesses and thick debris near the terminus leads to low, nearly uniform surface velocities, independent of climate change (Fig. 6). While it is possible that debris cover can produce low velocity portions of glaciers independent of climate change, periods of negative mass balance can also lead to extensive portions of debris-covered glaciers with low surface velocities due to the largest increases in melt rates occurring near $x_{\epsilon_{int}}$ (e.g., Kirkbride, 1993).

The ice discharge at the point of debris emergence, $x_{\epsilon_{int}}$, controls the steady state glacier length and the down glacier patterns of ice discharge, ice thickness and surface velocity. In steady state, ice discharge at $x_{\epsilon_{int}}$ represents the volume of ice per unit time that must be ablated between $x_{\epsilon_{int}}$ and the terminus. Holding other debris-related variables constant, if debris emerges where ice discharge is high, the glacier will extend further because more glacier surface under thick debris (where melt rates are low and more uniform) is needed for ablation and match the large ice discharge at $x_{\epsilon_{int}}$. If debris emerges where ice discharge is small the glacier does not extend as far because less area is needed under debris to match ice discharge at $x_{\epsilon_{int}}$ (Fig. 6). The location of debris deposition/emergence relative to the ELA is therefore an important variable in the debris-glacier system, as it controls the relationship between debris cover percentage, AAR, and the pattern of surface velocities (Fig. 11).

The specific terminal pattern of ice discharge and thickness is controlled by the rate of debris removal from the terminal wedge (Appendix A and B; Figs. A1 and B1). If $\dot{d}_{flux}^{term}$ is high, an ice cliff may persist at the toe leading to high melt rates and the pre-mature termination of a glacier when compared to a glacier with a low $\dot{d}_{flux}^{term}$. If the magnitude of $\dot{d}_{flux}^{term}$ is low then the toe may be drowned in debris, and the glacier may never reach steady state even with a steady climate. The glacier would continue to accumulate debris and slowly advance down valley with a slightly positive net mass balance (e.g., Konrad and Humphrey, 2000). It may be useful to consider if individual debris-covered glaciers are accumulating debris mass through time, losing debris mass through time, or potentially in quasi-steady state with regard to debris (Fig. 4).

The response time of the modeled glaciers is therefore dependent on the parameterization of $\dot{d}_{flux}^{term}$ (Appendix B). A glacier with rapid debris removal at the margin will tend to reach a steady state much faster than a glacier with slow debris removal from the margin (Appendix B). Documenting the rates of debris removal at the margin is therefore vital for modeling and understanding individual debris-covered glacier response.

In our steady state simulations, the ice thickness is increased up glacier from the point of debris emergence (Fig. 6). The thickness perturbations caused by emerging debris are diffused up glacier, leading to lower ice surface slopes and greater ice thicknesses than on debris-free glaciers forced by the same climate. The emergence of debris on a glacier can therefore perturb ice thickness both up and down glacier from the point of debris emergence. Debris cover decreases the surface mass balance and therefore also reduces the vertical component of englacial velocity; this leads to flow paths that are increasingly parallel to the surface (Konrad and Humphrey, 2000). Reducing ablation rates results in lower debris emergence rates, leading to the further advection of debris down glacier and expansion of the zone

of debris emergence (Fig. 5a). Debris emergence zones will therefore tend to be wider than debris deposition zones.

6 Potential model improvements and future research

While we have explored first-order connections between glacier dynamics and debris deposition, additional components require investigation. Modeling the response of debris-covered glaciers to climate is the most pressing (e.g., Naito et al., 2000; Banerjee and Shankar, 2013; Rowan et al., 2015). The steady state results presented here can serve as initial conditions for future simulations exploring the response of debris-covered glaciers to climate change. Future efforts should further explore the importance of glacier size, environmental mass balance gradient, and valley bedrock profile as they modulate the effect of debris on glacier response.

We assumed a steady debris input for simplicity. In reality, hillslope erosion in high-relief settings occurs through thresholded, mass wasting processes. The effect of temporal and spatial changes in debris deposition must be addressed through both empirical and theoretical approaches. Isolated, large landslides have been shown to suppress melt rates, change glacier surface slopes and perturb glacier surface velocity fields (Gardner and Hewitt, 1990; Reznichenko et al., 2011; Shugar et al., 2012). If debris inputs are allowed to vary in space and time, a complex glacier length history will likely result even with a steady climate. The specifics of that history will depend strongly on the frequency and magnitude of mass wasting events and to a lesser degree the ice discharge at the point of debris emergence.

Our modeling did not account for the plan-view dimension of glaciers. Debris advected into the glacier between tributaries emerges to form ice-stream interaction medial moraines. While the spatial widening of such moraines has been addressed (Anderson, 2000), the merging of these medial moraines results in debris thickening that we do not account for. Our present work lays the framework for such a 2-D plan-view model.

Ice cliffs, surface ponds, and proglacial lakes are neglected in this study for simplicity but should be included in numerical models of glacier response to debris and climate change (e.g., Benn et al., 2012). Plan-view modeling of debris-covered glacier response is also needed (e.g., Menounos et al., 2013; Rowan et al., 2015). The melt-enhancing effects of thin debris covers should be included in future modeling efforts. Environmental mass balance profiles and snow lines are not steady from year-to-year. The response of debris-covered glaciers to interannual climate variability must also be explored (Roe and O'Neal, 2009; Anderson et al., 2014). Debris covers and glacier lengths will fluctuate in response to this variability due to the feedbacks between the debris emergence, ice dynamics, and climate.

Debris advection through and on a glacier can take hundreds of years, leading to memory in the system (i.e., the glacier responds to debris input from hundreds of years ago).

The response of individual debris-covered glaciers to climate change is therefore dependent on the distribution of debris on and in the glacier when the climate change occurs. Further constraint of englacial and surface debris is needed to predict the decadal to centennial response of present debris-covered glaciers to climate change.

7 Conclusions

It is necessary to constrain the effect of debris on glaciers so we can better predict the response of debris-covered glaciers to climate change. We provide a new framework to explore debris-covered glacier evolution and explore valley glacier sensitivity to debris input. Our simulations show the following:

- For reasonable debris deposition fluxes, debris input can lead to glaciers that are many tens of percent longer than debris-free glaciers forced by the same climate but unperturbed by debris.

- Thick debris cover tends to reduce gradients of ice discharge, ice thickness, and surfaces velocities, independent of climate change.

- Debris-covered glacier length is highly sensitive to debris flux to the glacier surface. High surface debris fluxes can greatly increase glacier lengths relative to glaciers responding to the same climate without debris. Increases in debris flux lead to smaller AARs and larger debris covered fractions. Changes in the debris deposition zone width or the debris deposition rate are secondary to the total surface debris flux in governing the glacier geometry. This model provides a framework to quantify the effect of debris input on glacier length, and can therefore be used to estimate the effect of debris input on paleoclimate estimates derived from glacier models.

- The site of supraglacial debris deposition relative to the ELA modulates glacier response to debris. Steady debris input where ice discharge is high (near the ELA) leads to longer glaciers with greater fractional debris cover, whereas the same steady debris input where ice discharge is low (near the headwall or terminus) leads to shorter glaciers with smaller fractional debris cover.

- The importance of the mechanism of debris deposition onto glaciers (e.g., delivery by avalanching or by melt out of debris septa) is likely secondary to the importance of the total surface debris flux.

- Debris-covered glacier length is highly sensitive to the relationship between surface debris thickness and sub-debris melt. Our simulations support the use of capped hyperbolic debris thickness–melt curve fits (Eq. 3) instead of exponential fits.

– The rate and process of debris removal from the terminus exerts strong control on the time evolution of debris-covered glaciers, but only weakly influences the eventual steady-state length.

– Debris cover can perturb ice thicknesses and glacier surface slopes up glacier from the debris-covered portion of the glacier. Thick debris cover can expand the zone of debris emergence. Debris emergence zones will therefore be longer than zones of debris deposition.

Glacier response to debris cover is most sensitive to surface debris flux and the debris thickness–melt relationship. Our ability to predict the response of debris-covered glaciers to climate change, and to extract paleoclimate estimates from moraines in high-relief settings, is therefore highly dependent on our constraint of surface debris fluxes and debris thickness–melt relationship in the future and the past.
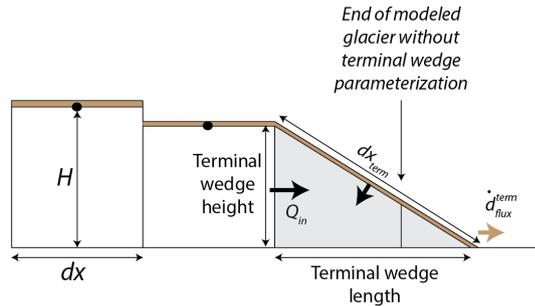
Figure A1. The terminal wedge parameterization and debris removal from the model. Q_{in} is the ice discharge into the terminal wedge. $\dot{d}_{\text{flux}}^{\text{term}}$ is removed from the total volume of surface debris on the terminal wedge.

Appendix A

After the step change increase in debris deposition occurs, the steady-state debris free glacier evolves towards a debris-covered steady state. During this transition debris on the glacier surface is advected from cells with debris cover into debris-free cells. In our model, the debris thickness $h_{\text{debris}}(x, t)$ represents a layer of equal thickness on any cell. Debris thickens more slowly with a larger dx because the debris volume advected into a cell is spread over a larger area (due to the larger dx; dy=1; dy (in m)). There is therefore a timescale built into the thickening of debris in a cell that is dependent on dx. Because ablation rates are sensitive to debris-cover thickness, changing dx has an effect on glacier evolution. In order to test the effect of changing dx on the steady state debris-covered glacier length we increased dx from 100 (used in all simulations outside of this test) to 200 m. This test led to differences in steady state debris-covered glacier length which were less than 200 m even when

$\dot{d}_{\text{flux}}$ was varied. The dx dependence does not effect the conclusions we draw from this study.

Without a terminus wedge parameterization, simulated glaciers advancing toward steady state become trapped in false steady states. Without a terminus wedge parameterization a new glacier cell is exposed to melt rates un-perturbed by debris. As a result, simulated glaciers become trapped in a steady length, even though large volumes of ice are melted without the protection of debris. To correct this, we implement a triangular terminal wedge parameterization for the last two grid points (the last ice-covered and the first ice-free grid point; Fig. A1; see Budd and Jenssen, 1975; Waddington, 1981) of the glacier which allows debris to cover the glacier terminus even when advancing or retreating. The volume and length of the terminal wedge is based on ice mass conservation. The volume of the terminal wedge at time $t+$dt is the sum of the old terminus volume, the ablated volume under debris, and the volumetric flow past the last grid point. Equation (16) and dx_{term}, the surface length of the wedge, define the debris thickness on the terminal wedge. $\dot{d}_{\text{flux}}^{\text{term}}$ removes debris from the total volume of debris on the terminal debris wedge. A single environmental melt rate is calculated based on the mean elevation of the terminal wedge, and sub-debris ablation is calculated perpendicular to the surface of the wedge. When the terminal wedge length is greater than 2dx, the wedge parameterization moves to the next cell down valley. If the terminal wedge is shorter than dx the terminal wedge parameterization retreats one cell. Because the terminus parameterization allows the glacier to change length at the sub-dx scale, simulated glaciers avoid numerical traps and advance to true steady states. In this model, steady state occurs when $\dot{d}_{\text{flux}} = \dot{d}_{\text{flux}}^{\text{term}}$ and the glacier length is steady.
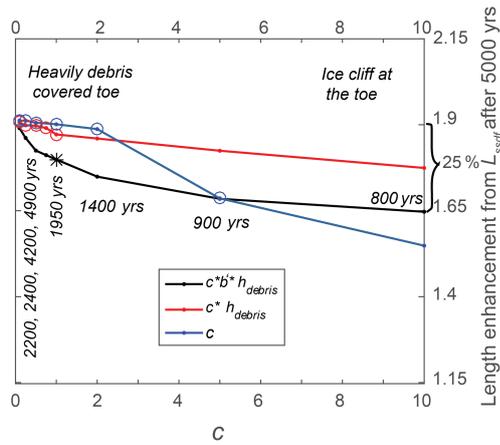
Figure B1. Exploring various choices for the $\dot{d}_{\text{flux}}^{\text{term}}$ parameterization. Glacier lengths are normalized by the steady state debris free glacier length (L_{ssdf}). Irrespective of the choice of the $\dot{d}_{\text{flux}}^{\text{term}}$ parameterization the steady glacier length is nearly doubled. For all simulations $\dot{d}_{\text{flux}}$ is 3.2 m³ m⁻¹ yr⁻¹. The glacier will never reach steady state for choices where $\dot{d}_{\text{flux}}^{\text{term}}$ cannot evolve to equal $\dot{d}_{\text{flux}}$. This occurs when $\dot{d}_{\text{flux}}^{\text{term}} = c$ and c is less than 3.2 m³ m⁻¹ yr⁻¹. Circles represent simulations in which M_{surface} (the total debris mass on the glacier) and glacier length did not reach steady state after 5000 years. The time labels show how long it took for the glacier to reach steady state for the cases when $\dot{d}_{\text{flux}}^{\text{term}} = c\dot{b}h_{\text{debris}}$. All simulations presented outside of this plot use the $\dot{d}_{\text{flux}}^{\text{term}} = c\dot{b}h_{\text{debris}}$ parameterization with $c = 1$ (∗ in this figure).

Appendix B

Debris deposited on the glacier surface is removed from the glacier by ice cliff retreat or wasting down the terminal glacier slope. Unfortunately, the rates and processes of debris removal from glacier toes are poorly documented. We therefore explore parameterizations for the debris removal

flux from the glacier ($\dot{d}_{\text{flux}}^{\text{term}}$) and their effect on glacier length (using the base parameter set where $\dot{d}_{\text{flux}} = 3.2$ m³ m⁻¹ yr⁻¹). Each simulation starts with the ssdf glacier followed by a step change increase in $\dot{d}_{\text{flux}}$. We consider $\dot{d}_{\text{flux}}^{\text{term}} = c$, $\dot{d}_{\text{flux}}^{\text{term}} = ch_{\text{debris}}$, and $\dot{d}_{\text{flux}}^{\text{term}} = c\dot{b}_z h_{\text{debris}}$ where c is a constant that ranges between 0.1 and 10 with variable units such that $\dot{d}_{\text{flux}}^{\text{term}}$ [in m³ m⁻¹ yr⁻¹]. Independent of the parameterization, $\dot{d}_{\text{flux}}^{\text{term}}$ controls both the time needed to reach steady state as well as whether a simulated glacier can reach steady state (Fig. B1).

Large changes in $\dot{d}_{\text{flux}}^{\text{term}}$ lead to minor changes in glacier length even after 5000 years, implying that the choice of the $\dot{d}_{\text{flux}}^{\text{term}}$ parameterization would have a minor effect on the length results presented (Fig. B1). All three parameterizations lead to the same steady state length for low c values (190 % of L_{ssdf}).

If $\dot{d}_{\text{flux}}^{\text{term}}$ cannot evolve to a state where $\dot{d}_{\text{flux}}^{\text{term}} = \dot{d}_{\text{flux}}$, surface debris thickens unrealistically and the glacier never reaches steady state. For $\dot{d}_{\text{flux}}^{\text{term}} = c$ the glacier will never reach steady state if c is less than 3.2 m³ m⁻¹ yr⁻¹. For $\dot{d}_{\text{flux}}^{\text{term}} = ch_{\text{debris}}$, and $\dot{d}_{\text{flux}}^{\text{term}} = c\dot{b}_z h_{\text{debris}}$ the value of $\dot{d}_{\text{flux}}^{\text{term}}$ changes through each simulation based on the debris thickness on the toe and the local debris-free melt rate. The $\dot{d}_{\text{flux}}^{\text{term}} = c\dot{b}_z h_{\text{debris}}$ parameter shows a wider length variation than the $\dot{d}_{\text{flux}}^{\text{term}} = ch_{\text{debris}}$ parameterization because $\dot{d}_{\text{flux}}^{\text{term}} = c\dot{b}_z h_{\text{debris}}$ results in a wider range of $\dot{d}_{\text{flux}}^{\text{term}}$ values due to the $\dot{b}_z$ term. To ensure that steady state can be achieved in each simulation, we include the melt rate term in the $\dot{d}_{\text{flux}}^{\text{term}}$ parameterization (Fig. B1) that codifies an assumption that debris removal processes at the toe are in some fashion dependent on local air temperature and hence melt rates. We use $\dot{d}_{\text{flux}}^{\text{term}} = c\dot{b}_z h_{\text{debris}}$ for all simulations outside of this Appendix (with $c = 1$).

References

Anderson, L. S.: Glacier response to climate change: modeling the effects of weather and debris-cover, PhD thesis, University of Colorado, Boulder, 175 pp., 2014.

Anderson, L. S., Roe, G. H., and Anderson, R. S.: The effects of interannual climate variability on the moraine record, Geology, 42, 55–58, 2014.

Anderson, R. S.: A model of ablation-dominated medial moraines and the generation of debris-mantled glacier terms, J. Glaciol., 46, 459–469, doi:10.3189/172756500781833025, 2000.

Arsenault, A. M. and Meigs, A. J.: Contribution of deep-seated bedrock landslides to erosion of a glaciated basin in southern Alaska, Earth Surf. Proc. Land., 30, 1111–1125, doi:10.1002/esp.1265, 2005.

Ballantyne, C. K. and Harris, C.: The Periglaciation of Great Britain, Cambridge University Press, Cambridge, UK, 335 pp., 1994.

Banerjee, A. and Shankar, R.: On the response of Himalayan glaciers to climate change, J. Glaciol., 59, 480–490, 2013.

Benn, D. and Evans, D. J. A.: Glaciers and Glaciation, Routledge, London, UK, 802 pp., 2010.

Benn, D. I. and Owen, L. A.: Himalayan glacial sedimentary environments: a framework for reconstructing and dating the former extent of glaciers in high mountains, Quatern. Int., 97–98, 3–25, doi:10.1016/S1040-6182(02)00048-4, 2002.

Benn, D., Bolch, T., Hands, K., Gulley, J., Luckman, A., Nicholson, L., Quincey, D., Thompson, S., Toumi, R., and Wiseman, S.: Response of debris-covered glaciers in the Mount Everest region to recent warming, and implications for outburst flood hazards, Earth-Sci. Rev., 114, 156–174, doi:10.1016/j.earscirev.2012.03.008, 2012.

Bolch, T., Pieczonka, T., and Benn, D. I.: Multi-decadal mass loss of glaciers in the Everest area (Nepal Himalaya) derived from stereo imagery, The Cryosphere, 5, 349–358, doi:10.5194/tc-5-349-2011, 2011.

Bolch, T., Kulkarni, A. and Kääb, A., Huggel, C., Paul, F., Cogley, J. G., Frey, H., Kargel, J. S., Fujita, K., Scheel, M., Bajracharya, S. and Stoffel, M.: The State and Fate of Himalayan Glaciers, Science, 336, 310–314, doi:10.1126/science.1215828, 2012.

Boulton, G. S. and Eyles, N.: Sedimentation by valley glaciers: a model and genetic classification, Moraines and Varves, 33, 11–23, 1979.

Bozhinskiy, A. N., Krass, M. S., and Popovnin, V. V.: Role of debris cover in the thermal physics of glaciers, J. Glaciol., 32, 255–266, 1986.

Brook, M., Hagg, W., and Winkler, S.: Debris cover and surface melt at a temperate maritime alpine glacier: Franz Josef Glacier, New Zealand, New Zeal. J. Geol. Geop., 56, 27–38, doi:10.1080/00288306.2012.736391, 2013.

Budd, W. and Jenssen, D.: Numerical modelling of glacier systems, IAHS-AISH P., 104, 257–291, 1975.

Clark, D. H., Clark, M. M., and Gillespie, A. R.: Debris-covered glaciers in the Sierra Nevada, California, and their implications for snowline reconstructions, Quaternary Res., 41, 139–153, 1994.

Conway, H. and Rasmussen, L. A.: Summer temperature profiles within supraglacial debris on Khumbu Glacier, Nepal, in: Debris-covered Glaciers: Proceedings of an International Workshop Held at the University of Washington in Seattle, Washington, USA, 13–15 September 2000, IAHS Publication 264, p. 289, 2000.

Cuffey, K. and Paterson, W.: The Physics of Glaciers, Elsevier, Oxford, UK, 4th edn., 704 pp., 2010.

Deline, P.: Interactions between rock avalanches and glaciers in the Mont Blanc massif during the late Holocene, Quaternary Sci. Rev., 28, 1070–1083, doi:10.1016/j.quascirev.2008.09.025, 2009.

Eyles, N. and Rogerson, R. J.: A framework for the investigation of medial moraine formation: Austerdalsbreen, Norway, and Berendon Glacier, British Columbia, Canada, J. Glaciol., 20, 99–113, 1978.

Fyffe, C. L.: The hydrology of debris-covered glaciers, PhD thesis, University of Dundee, UK, 352 pp., 2012.

Gardner, J. S. and Hewitt, K.: A surge of Bualtar Glacier, Karakoram Range, Pakistan: a possible landslide trigger, J. Glaciol., 36, 159–162, 1990.

Hagg, W., Mayer, C., Lambrecht, A., and Helm, A.: Sub-debris melt rates on Southern Inylchek Glacier, Central Tian Shan, Geogr. Ann. A, 90, 55–63, 2008.

Hambrey, M. J. and Quincey, D. J., Glasser, N. F., Reynolds, J. M., Richardson, S. J. and Clemmens, S.: Sedimentological, geomorphological and dynamic context of debris-mantled glaciers, Mount Everest (Sagarmatha) region, Nepal, Quaternary Sci. Rev., 27, 2361-2389, 2008.

Heimsath, A. M. and McGlynn, R.: Quantifying periglacial erosion in the Nepal high Himalaya, Geomorphology, 97, 5–23, doi:10.1016/j.geomorph.2007.02.046, 2008.

Hooke, R. L. and Hudleston, P. J.: Origin of foliation in glaciers, J. Glaciol., 20, 285–299, 1978.

Humlum, O.: The geomorphic significance of rock glaciers: estimates of rock glacier debris volumes and headwall recession rates in West Greenland, Geomorphology, 35, 41–67, 2000.

Humlum, O.: Holocene permafrost aggradation in Svalbard, Geological Society, London, Special Publications, 242, 119–129, doi:10.1144/GSL.SP.2005.242.01.11, 2005.

Kääb, A., Berthier, E., Nuth, C., Gardelle, J. and Arnaud, Y.: Contrasting patterns of early twenty-first-century glacier mass change in the Himalayas, Nature, 488, 495-498, 2012.

Kayasha, R., Takeuchi, Y., Nakawo, M., and Ageta, Y.: Practical prediction of ice melting beneath various thicknesses of debris cover on Kumbu Glacier, Nepal, using a positive degree-day factor, in: Debris-covered Glaciers: Proceedings of an International Workshop Held at the University of Washington in Seattle, Washington, USA, 13–15 September 2000, IAHS Publication 264, p. 289, 2000.

Kessler, M. A., Anderson, R. S., and Stock, G. M.: Modeling topographic and climatic control of east-west asymmetry in Sierra Nevada glacier length during the Last Glacial Maximum, J. Geophys. Res., 111, F02002, doi:10.1029/2005JF000365, 2006.

Khan, M. I.: Ablation on Barpu glacier, Karakoram Himalaya, Pakistan a study of melt processes on a faceted, debris-covered ice surface, PhD thesis, Wilfrid Laurier University, USA, 1989.

Kirkbride, M. P.: The temporal significance of transitions from melting to calving termini at glaciers in the central Southern Alps of New Zealand, Holocene, 3, 232–240, doi:10.1177/095968369300300305, 1993.

Kirkbride, M. P.: Debris-covered glaciers, in: Encyclopedia of snow, ice and glaciers, edited by: Singh, V., Singh, P., and Haritashya, U. K., Springer, Dordrecht, 190–191, 2011.

Kirkbride, M. P. and Deline, P.: The formation of supraglacial debris covers by primary dispersal from transverse englacial debris bands, Earth Surf. Proc. Land., 38, 1779–1792, doi:10.1002/esp.3416, 2013.

Konrad, S. K. and Humphrey, N. F.: Steady-state flow model of debris-covered glaciers (rock glaciers), in: Debris-covered Glaciers: Proceedings of an International Workshop Held at the University of Washington in Seattle, Washington, USA, 13–15 September 2000, 255–266, 2000.

Leysinger Vieli, G. J. M. C. and Gudmundsson, G. H.: On estimating length fluctuations of glaciers caused by changes in climatic forcing, J. Geophys. Res., 109, 1-14, 2004.

Loomis, S. R.: Morphology and ablation processes on glacier ice. Part 1, Morphology and structure of an ice-cored medial moraine, Kaskawulsh Glacier, Yukon, Arctic Institute of North America, Research Paper, 1–65, 1970.

Lukas, S., Nicholson, L. I., Ross, F. H., and Humlum, O.: Formation, meltout processes and landscape alteration of high-Arctic ice-cored moraines examples from Nordenskiold Land, Central Spitsbergen, Polar Geography, 29, 157–187, doi:10.1080/789610198, 2005.

Lundstrom, S. C.: The budget and effect of superglacial debris on Eliot Glacier, Mount Hood, Oregon, PhD thesis, University of Colorado, Boulder, 183 pp., 1993.

MacGregor, K. R., Anderson, R. S., and Waddington, E. D.: Numerical simulations of glacial-valley longitudinal profile evolution, Geology, 28, 1031–1034, 2000.

Marshall, S. J., Bjornsson, H., Flowers, G. E., and Clarke, G. K. C.: Simulation of Vatnajökull ice cap dynamics, J. Geophys. Res., 110, 126–135, doi:10.1029/2004JF000262, 2005.

Mattson, L. E., Gardner, J. S., and Young, G. J.: Ablation on debris covered glaciers: an example from the Rakhiot Glacier, Punjab, Himalaya, in: Snow and Glacier Hydrology (Proceedings of the Kathmandu Symposium), Kathmandu, November 1992, IAHS Publication, 218, 289–296, 1993.

Meier, M. and Post, A.: Recent Variations in mass net budgets of glaciers in western North America, IASH-AISH P., 58, 63–77, 1962.

Menounos, B., Clague, J. J., Clarke, G. K. C., Marcott, S. A., Osborn, G., Clark, P. U., Tennant, C., and Novak, A. M.: Did rock avalanche deposits modulate the late Holocene advance of Tiedemann Glacier, southern Coast Mountains, British Columbia, Canada?, Earth Planet. Sc. Lett., 384, 154–164, 2013.

Messerli, B. and Zurbuchen, M.: Block-gletscher im Weissmies und Aletsch und ihre photogrammetrische Kartierung, Die Alpen, 3, 139–152, 1968.

Mihalcea, C., Mayer, C., Diolaiuti, G., Lambrecht, A., Smiraglia, C., and Tartari, G.: Ice ablation and meteorological conditions on the debris-covered area of Baltoro glacier, Karakoram, Pakistan, Ann. Glaciol., 43, 292–300, 2006.

Molnar, P., Anderson, R. S., and Anderson, S. P.: Tectonics, fracturing of rock, and erosion, J. Geophys. Res.-Earth, 112, 1–12, doi:10.1029/2005JF000433, 2007.

Naito, N., Nakawo, M., Kadota, T., and Raymond, C. F.: Numerical simulation of recent shrinkage of Khuinbu Glacier, Nepal Himalayas, in: Debris-covered Glaciers: Proceedings of an International Workshop Held at the University of Washington in Seattle, Washington, USA, 13–15 September 2000, 264, p. 245, IAHS, 2000.

Nicholson, L. and Benn, D. I.: Calculating ice melt beneath a debris layer using meteorological data, J. Glaciol., 52, 463–470, 2006.

Nye, J. F.: A numerical method of inferring the budget history of a glacier from its advance and retreat, J. Glaciol., 5, 589–607, 1965.

Østrem, G.: Ice melting under a thin layer of moraine, and the existence of ice cores in moraine ridges, Geogr. Ann. Ser. A, Phys. Geogr., 228–230, 1959.

Oerlemans, J.: An attempt to simulate historic front variations of Nigardsbreen, Norway, Theor. Appl. Climatol., 135, 126–135, 1986.

O'Farrell, C. R. O., Heimsath, A. M., Lawson, D. E., Jorgensen, L. M., Evenson, E. B., Larson, G., and Denner, J.: Quantifying periglacial erosion: insights on a glacial sediment budget, Matanuska Glacier, Alaska, Earth Surf. Proc. Land., 34, 2008–2022, 2009.

Ouimet, W. B., Whipple, K. X., and Granger, D. E.: Beyond threshold hillslopes: channel adjustment to base-level fall in tectonically active mountain ranges, Geology, 37, 579–582, doi:10.1130/G30013A.1, 2009.

Owen, L. A. and Derbyshire, E.: The Karakoram glacial depositional system, Z. Geomorphol. Supp., 76, 33–73, 1989.

Owen, L. A., Derbyshire, E., and Scott, C. H.: Contemporary sediment production and transfer in high-altitude glaciers, Sediment. Geol., 155, 13–36, 2003.

Raper, S. C. B. and Braithwaite, R. J.: Low sea level rise projections from mountain glaciers and icecaps under global warming, Nature, 439, 311–313, doi:10.1038/nature04448, 2006.

Reid, T. D. and Brock, B. W.: An energy-balance model for debris-covered glaciers including heat conduction through the debris layer, J. Glaciol., 56, 903–916, doi:10.3189/002214310794457218, 2010.

Reid, T. D. and Brock, B. W.: Assessing ice-cliff backwasting and its contribution to total ablation of debris-covered Miage glacier, Mont Blanc massif, Italy, J. Glaciol., 60, 3–13, 2014.

Reznichenko, N. V., Davies, T. R. H., and Alexander, D. J.: Effects of rock avalanches on glacier behaviour and moraine formation, Geomorphology, 132, 327–338, doi:10.1016/j.geomorph.2011.05.019, 2011.

Roe, G. H. and Neal, M. A. O.: The response of glaciers to intrinsic climate variability: observations and models of late-Holocene variations in the Pacific Northwest, J. Glaciol., 55, 839–854, 2009.

Rowan, A. V., Egholm, D. L., Quincey, D. J. and Glasser, N. F.: Modelling the feedbacks between mass balance, ice flow and debris transport to predict the response to climate change of debris-covered glaciers in the Himalaya, Earth Planet. Sci. Lett., 430, 427-438, doi:10.1016/j.epsl.2015.09.004, 2015.

Scherler, D.: Climatic limits to headwall retreat in the Khumbu Himalaya, eastern Nepal, Geology, doi:10.1130/G35975.1, 2014.

Scherler, D., Bookhagen, B., and Strecker, M. R.: Spatially variable response of Himalayan glaciers to climate change affected by debris cover, Nat. Geosci., 4, 156–159, doi:10.1038/ngeo1068, 2011a.

Scherler, D., Bookhagen, B., and Strecker, M. R.: Hillslope-glacier coupling: the interplay of topography and glacial dynamics in High Asia, J. Geophys. Res., 116, F02019, doi:10.1029/2010JF001751, 2011b.

Shea, J. M., Immerzeel, W. W., Wagnon, P., Vincent, C., and Bajracharya, S.: Modelling glacier change in the Everest region, Nepal Himalaya, The Cryosphere, 9, 1105–1128, doi:10.5194/tc-9-1105-2015, 2015.

Shroder, J. F., Shroder, J. F., Bishop, M. P., Bishop, M. P., Copland, L., Copland, L., Sloan, V. F., and Sloan, V. F.: Debris-covered glaciers and rock glaciers in the Nanga Parbat Himalaya, Pakistan, Geogr. Ann. A, 82, 17–31, doi:10.1111/j.0435-3676.2000.00108.x, 2000.

Shugar, D. H., Rabus, B. T., Clague, J. J., and Capps, D. M.: The response of Black Rapids Glacier, Alaska, to the Denali earthquake rock avalanches, J. Geophys. Res.-Earth, 117, 1–14, doi:10.1029/2011JF002011, 2012.

Smolarkiewicz, P. K.: A simple positive definite advection scheme with small implicit diffusion, Mon. Weather Rev., 111, 479–486, 1983.

Stock, J. D. and Montgomery, D. R.: Geologic constraints on bedrock river incision using the stream power law, J. Geophys. Res., 104, 4983, doi:10.1029/98JB02139, 1999.

Vacco, D. A., Alley, R. B., and Pollard, D.: Glacial advance and stagnation caused by rock avalanches, Earth Planet. Sc. Lett., 294, 123–130, doi:10.1016/j.epsl.2010.03.019, 2010.

Waddington, E. D.: Accurate modelling of glacier flow, PhD thesis, University of British Columbia, Canada, 460 pp., 1981.

Wagnon, P., Vincent, C., Arnaud, Y., Berthier, E., Vuillermoz, E., Gruber, S., Ménégoz, M., Gilbert, A., Dumont, M., Shea, J. M., Stumm, D., and Pokhrel, B. K.: Seasonal and annual mass balances of Mera and Pokalde glaciers (Nepal Himalaya) since 2007, The Cryosphere, 7, 1769–1786, doi:10.5194/tc-7-1769-2013, 2013.

Wang, L., Li, Z., and Wang, F.: Spatial distribution of the debris layer on glaciers of the Tuomuer Peak, western Tian Shan, J. Earth Sci., 22, 528–538, doi:10.1007/s12583-011-0205-6, 2011.

Ward, D. J. and Anderson, R. S.: The use of ablation-dominated medial moraines as samplers for 10Be-derived erosion rates of glacier valley walls, Kichatna Mountains, AK, Earth Surf. Proc. Land., 36, 495–512, doi:10.1002/esp.2068, 2011.

WGMS: Global glacier changes: facts and figures, edited by: Zemp, M., Roer, I., Kääb, A., Hoelzle, M., Paul, F., and Haerberli, W., UNEP, World Glacier Monitoring Service, Zürich, 45 pp., 2008.